Tribology International 173 (2022) 107649

Contents lists available at ScienceDirect

Tribology International

journal homepage: www.elsevier.com/locate/triboint

On the role of strain hardening and mechanical properties in water droplet erosion of metals

Rizwan Ahmed Shaik, Mohamed Elhadi Ibrahim, Abdullahi Kachalla Gujba, Martin David Pugh, Mamoun Medraj *

Department of Mechanical, Industrial and Aerospace Engineering, Concordia University, Montreal, Quebec H3G 1M8, Canada

ARTICLE INFO

Keywords:
Water droplet erosion
Strain hardening
Mechanical properties
17–4 PH stainless steel

ABSTRACT

The role of strain hardening on the resistance of metals to water droplet erosion is investigated for the first time. A stainless steel (17–4PH) was heat treated to various conditions to achieve different sets of mechanical properties. Erosion tests were then performed at 250 and 300 m/s impact speeds and incubation time and erosion rate were measured. It was found that higher strain hardening is conducive to higher erosion resistance as demonstrated by longer incubation time. Strain hardening was also found to dictate the influence of other mechanical properties, such as yield strength and resilience, on the initial stages of erosion. It is concluded that erosion resistance is a synergistic combination of mechanical properties that includes a stain hardening parameter.

1. Introduction

Water droplet erosion (WDE) is a form of material wear caused by the repetitive impingements of liquid droplets on solid surfaces. WDE damage is mostly seen on blades of gas, steam, and wind turbines [1,2] where it poses a serious reliability concern. For this reason, understanding the fundamental aspects of droplet impact damage and developing practical solutions to the problem are subjects of intensive recent investigations [3–8].

The fundamental studies of WDE focus on (i) understanding the physics surrounding the high-strain-rate liquid-solid interaction taking place during single droplet impact event and on (ii) the mechanics of damage accumulation due to the repetitive impacts [9]. In the case of a single droplet impact event, it is so far known that the impingement of a liquid droplet on a solid surface results in a high contact pressure (known as water hammer pressure) [10]. Water hammer pressure, then, acts as a dynamic loading parameter -over a certain duration- with which the droplet induces stresses on the solid target by means of stress wave propagation [11]. As the duration of impact pressure ends and the pressurized liquid starts releasing, the droplet spreads away and forms sideways jets that also subject the surface to shear stresses [9]. There is no evidence that the two stress components (i.e. direct stress from impact pressure and shear stress from lateral jetting) overlap and superimpose to result in greater magnitude of overall stress. It is known however that single droplet impact seldom causes detectable damage on the solid surface, and erosion in almost all cases is a product of repetitive impingements of multiple droplets in a fatigue-like fashion [8].

The mechanics of damage accumulation due to repetitive impacts are still poorly understood. Empirically, it has been observed [12] that initial droplet impingements result in the plastic deformation of the surface. During this stage (commonly referred to as the incubation period), only an increase in surface roughness is seen without noticeable erosion damage. Subsequent impingements of the surface results in large erosion pits that indicate the beginning of material damage (end of the incubation period). Once started, the erosion damage in terms of mass loss proceeds linearly with continuous exposure to droplet impacts in what is commonly referred to as steady-state maximum erosion rate stage. Though other stages of droplet impact erosion exist, the incubation period and the steady-state erosion rate are often considered the most important stages in water droplet erosion [13].

In both aspects of WDE (i.e. physics of single impact and mechanics of damage accumulation due to repetitive impacts), mechanical properties of the solid target play a fundamental role. In single impact event, even though the magnitude of the water hammer pressure is considered to be independent of the target properties, stresses generated from the pressure largely depend on the density, elastic modulus, sound and waves speed of the solid [11]. The work of Blowers [14], for example, analytically demonstrated how the response of an elastic solid to a droplet impact is dictated by the elastic modulus, sound and wave properties of the solid. The role of the mechanical properties appears to

* Corresponding author.
E-mail address: mmedraj@encs.concordia.ca (M. Medraj).

https://doi.org/10.1016/j.triboint.2022.107649
Received 18 March 2022; Received in revised form 27 April 2022; Accepted 17 May 2022
Available online 20 May 2022

be more significant with the case of the repetitive multiple impacts.

Many studies attempted to identify the mechanical properties that are fully responsible or partially contributing to the materials' resistance to water droplet erosion. Attempts to correlate materials' erosion resistance to individual-intrinsic properties such as hardness, fracture toughness, fatigue strength, and tensile properties have been made. Hardness received considerable attention due the fact that it successfully indicates the ability of metallic surfaces to resist other wear phenomena. For instance, some studies [12] showed that resistance to water droplet erosion is proportional to hardness raised to the power 2. However, Ahmad et al. [15] have recently demonstrated how hardness corelates to erosion resistance when different alloys are considered. The role of fracture toughness in water droplet erosion was also studied [16,17]. However, this was only for ceramic materials.

Studies aiming to correlate erosion resistance of metallic materials to fatigue properties were also reported in the literature [18,19]. This was mainly motivated by the analogy between water droplet erosion and fatigue, particularly in the damage accumulation aspect of the two phenomena. However, recent studies [20,21] have applied surface treatments to metallic samples, which are known inhibitors of fatigue, in order to delay erosion. It was concluded that fatigue is not a predominantly contributing erosion mechanism as no improvements in erosion performance were observed due to surface treatments. It was reasoned that the embrittlement due to strain hardening from surface treatments negates the beneficial effects of fatigue crack inhibiting compressive residual stresses. It is therefore imperative to study the role of strain hardening. Also, Adler [11] concluded from microscopic observation that fatigue could play only a secondary role at moderate to high impact velocities in metals. He [11] proposed that hydraulic penetration and tunneling are the predominant mechanism. Moreover, fatigue properties (e.g., endurance limit, fatigue strength, etc.) are difficult to precisely quantify for certain materials. For these reasons, correlating erosion resistance to fatigue properties is not always appropriate.

The role of tensile properties (such as yield, tensile, and fracture strength) on the erosion resistance of metallic materials have also been considered. These properties along with the stress-strain curve are seen as particularly significant when plastic strain accumulation is considered as the mechanism leading to erosion. Early investigations in this direction have focused on the individual tensile properties. For instance, the work of Hoff et al. [22] concluded that erosion resistance of metals is proportional to the ultimate tensile strength raised to the power of 1.8. Yield strength has also been considered in the work of Thiruvengadam et al. [23]. It has increasingly become evident that a combination of properties rather than an individual property is more representative to erosion resistance of metals. In this regard, strain energy and resilience have received considerable attention. Thiruvengadam [18] was the first to conclude that erosion rate in both cavitation and liquid impingement is inversely proportional to strain energy to fracture. On the other hand, both ultimate and elastic resilience have been considered. Hobbs [24] for example, found that ultimate resilience fits erosion resistance of metals more accurately than strain energy or tensile strength alone. The more recent work of Ahmad [15] argued that elastic resilience best fits erosion resistance of several metals such as stainless steel and titanium alloys.

The previous attempts to investigate the role of tensile properties on the erosion response (incubation period and/or steady-state erosion rate) overlooked two important aspects: (i) the role of the grain size and (ii) the influence of strain hardening on the process of damage accumulation. Even with comparable properties, grain size influences the erosion response of materials [25,26]. Nonetheless, most previous studies [15,22,23,27] utilized data (both erosion test results and mechanical properties) of various metallic alloys that have different grain sizes.

The role of strain hardening in water droplet erosion has not been taken into consideration in previous studies. Given the repetitive nature of the WDE problem, the strain hardening rate of the material is likely to influence the damage accumulation process, and hence, the erosion response of the materials. In some studies [22], it has been shown that hardness increases steadily (i.e., work hardening) during the incubation period due to droplet impacts. This impact hardening process depends on the strain hardening properties of the material. At the same time, as the hardness change, the instantaneous erosion resistance of metals also changes, which influences the damage accumulation process. As such, the strain hardening exponent of the material might have a strong influence on the length of the incubation period. This has not been studied before. To investigate the role of strain hardening in water droplet erosion, a suitable material must be selected. Such material or set of materials should offer variation in tensile properties with a range of strain hardening behaviors, while exhibiting minimal to no difference in the grain size, which is known to influence erosion [25,26]. This can best be achieved through selecting a single material that is then heat treated at different conditions to achieve precipitation hardening. Precipitation hardenable alloys such as 17–4 PH, 17–7 PH stainless steels and Copper-Beryllium alloys offer the possibility of changing the mechanical properties without changing the grain structure.

The present work aims to investigate the role of strain hardening along with the known influencers of erosion i.e., mechanical properties like yield strength, hardness and elastic resilience. 17–4 PH stainless steel that can offer a range of strain hardening exponents (n) and mechanical properties without significantly changing the grain structure as it is precipitation strengthened is carefully selected. The mechanical properties are quantified using tensile test and Vickers hardness. Erosion tests are then performed using an advanced erosion test rig. The influence of strain hardening, strength and elastic resilience on the incubation period and steady-state erosion rate are qualitatively analyzed.

2. Experimental procedure

2.1. Material and heat treatment

17–4 PH stainless steel is selected for the present study. This is because it is a commonly used blade material in steam and gas turbines, which are subject to water droplet erosion. More importantly, it has relatively simpler heat treatment procedures [28] that provide a wide range of properties. That is, the formation of copper-rich precipitates within the laths of martensitic matrix of the 17–4 PH stainless steel enables variation in strain hardening and mechanical properties [29–31] while the grain size remains the same.

Plates of 17–4 PH (with a chemical composition of about 17% chromium, 4% nickel and 4% copper) have been obtained in the solution treated condition. The as-received solution treated condition will be referred to as 'Condition-A′. Then, two aged conditions are used in this work; namely H925 and H1025. These conditions are achieved by aging the Condition-A for 4 h at 495 °C and 550 °C, respectively, followed by air cooling. ASTM A693 standard [28] is followed for the precipitation hardening treatments of 17–4 PH stainless steel.

2.2. Microstructure and surface characterization

Prior to erosion testing, microstructure and surface characterization has been performed on the three conditions of the 17–4 PH. This was done mainly to identify any variation in the grain structure and/or in the surface conditions that may influence the erosion performance of the alloys. Scanning electron microscope (SEM) (Hitachi S-3400N) was used to examine Condition-A, H925 and H1025 conditions. Back Scattered Electrons (BSE) mode was utilized to observe the cross-section of each condition. Samples in each condition were prepared by sectioning, polishing and etching them with Fry's reagent. Confocal laser scanning microscope (Olympus LEXT OLS4100) with a resolution of 10 nanometers was also used to measure the surface roughness of the samples. A representative area of 1225 μm x 1225 μm was selected from each sample surface. For each sample, average line roughness (Ra)

measurements were taken from 20 random lines and their mean value is calculated.

Fig. 1 shows that equiaxed martensitic grains of about 30–50 μm are observed in each condition of 17–4 PH stainless steel. In other words, no significant changes in grain size were observed due to aging treatments. This is in accordance with previous studies [29,30] where the formation of copper rich precipitates of the order of 10–20 nm within the martensitic matrix is known to cause variation in the mechanical properties without noticeable changes in the grain structure.

An average line surface roughness prior to erosion testing of each condition is calculated from roughness measurements along 20 sampling lines for each sample which was progressively ground to a 1200grit finish before taking the surface measurements. The average surface roughness of the samples is found to be consistent at about 0.012 μm with a standard deviation of 0.002 μm. This also demonstrates the consistency of the surface preparation process. Similar surface roughness among the samples is ascertained as different surface roughness may change the erosion incubation time for the same impact conditions [32].

In the absence of observable microstructural changes and surface roughness variations among the studied conditions of the 17–4 PH, any difference in the erosion performance can only be attributed to the variation in the mechanical properties. This the motivation of this study and was not taken into consideration in previous investigations.

2.3. Evaluation of mechanical properties

The mechanical properties in this work are assessed principally through tensile and hardness test.

2.3.1. Hardness test

Surface microhardness of 17–4 PH stainless steel of each condition having a 1200 grit surface finish was measured prior to the erosion tests using microhardness testing machine (Mitutoyo MVK-H1). A 500-gf load was applied for a duration of 15 s for each measurement. An average of ten readings was taken for each sample.

2.3.2. Tensile test

A universal testing machine (Instron-3382) was used to carry out tensile tests. Tensile dog-bone specimens were first machined according to the ASTM E8/E8M standard [33] in Condition-A. Some of the specimens were then heat treated to H925 and H1025 conditions. The samples were pulled at a crosshead speed of 1 mm/minute which amounts to a strain rate of about 0.003/minute. Two samples were tested at each condition to ascertain the repeatability of the results. Stress-strain curve for each condition is constructed, where the elastic modulus, 0.2% yield strength, tensile strength, elastic resilience, and strain hardening exponent are obtained. Elastic resilience is calculated by measuring the area under the elastic region of the engineering stress versus engineering strain curves whereas the strain hardening exponent and strength coefficient are calculated using Hollomon's equation, as reported in the literature for this material [34,35].

2.4. Water droplet erosion tests

Water droplet erosion tests were carried out on an advanced erosion test rig at Concordia University, Montreal, Canada, in accordance with the ASTM G73 standard [36]. A schematic of the water droplet erosion rig is shown in Fig. 2(a). The rig consists of an 18-inch rotating disc on which a pair of sample holders is mounted. The disc is placed horizontally in an air-tight chamber, where a vacuum pressure of 30–50 mbar is attained. The vacuum reduces the air friction and eventual rise in the temperature of the test chamber, which could lead to droplet evaporation. Rotational speeds of up to 20,000 rpm which corresponds to a linear impact speed of about 500 m/s can be achieved on this rig. Water droplets are introduced to the test chamber through a nozzle that is placed immediately above the surface of the test sample.

The 17–4 PH samples in each condition were machined to the test coupon shape and the test surface of each was finished using a 1200 grit SiC paper. The coupons are mounted on the sample holder as shown in Fig. 2(b). The sample-holder is then fixed on the disc of the erosion test

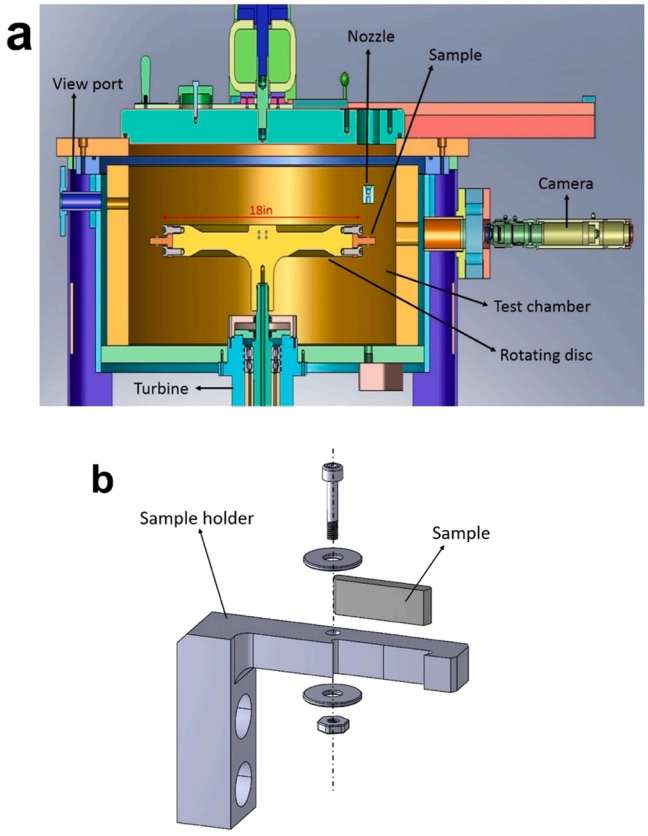

Fig. 2. (a) schematic of erosion test rig and (b) components of the sample holder assembly.

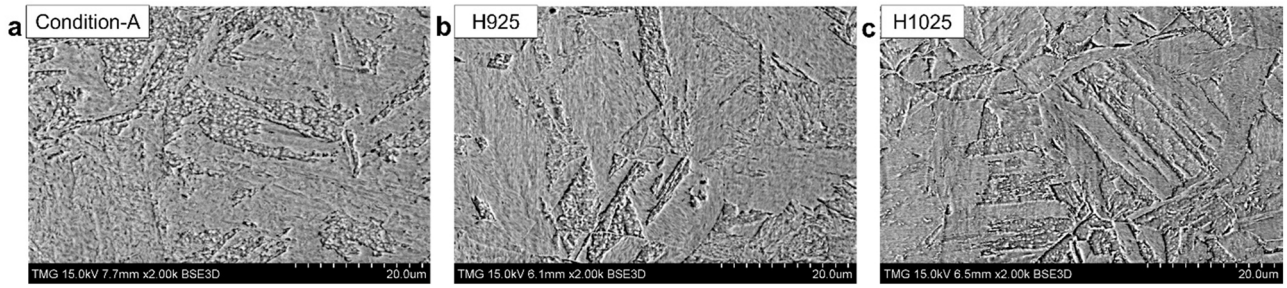

Fig. 1. SEM micrographs of the test conditions (a) Condition-A, (b) H925 and (c) H1025.

rig. The disc is driven by an air turbine. After the desired speed (test impact velocity) is achieved, water droplets (having an average size of 460 μm and a droplet count of 6 per the sample width of 8 mm each rotation upon impact [21,32]) are introduced through the nozzle. The droplets impact the surface of samples at 90° impact angle, which is the most severe impact angle for droplet erosion [37], where the erosion is more pronounced and hence making differences apparent. The erosion test parameters used in this study are summarized in Table 1.

The erosion test is periodically interrupted to track the erosion mass loss as it progresses with time. Samples are weighed after each cycle of testing on a balance with ± 0.0001 g accuracy. The measured mass loss and exposure time are used to plot the cumulative mass loss versus exposure time curve (i.e. erosion curve) for each test. Two important erosion responses are then extracted from the erosion curve; (i) the incubation period, which indicates the exposure duration needed to start the mass loss, and (ii) the steady-state maximum erosion rate, which is represented by the linear portion of the erosion curve.

Two identical 17–4 PH samples in Condition-A were initially tested to examine the consistency of the tested materials and the repeatability of the erosion results. These initial tests were done at two impact velocities: 250 and 300 m/s. The difference in mass loss after 40 and 250 min of exposure to droplet impact, for respective impact velocity, as well as the difference in the steady-state maximum erosion rate were evaluated. The uncertainty ranges for 250 and 300 m/s are summarized in Table 2. It can be seen from Table 2 that the maximum difference in the mass loss is found to be about 2 and 1.1 mg at 250 and 300 m/s, respectively. The difference in maximum erosion rate was found to be about 0.05 mg/min at each speed. Moreover, the erosion curves were observed to be repeatable and this demonstrates the uniformity in conditions and hence making the erosion performance of samples comparable. The relationship between the observed mechanical attributes and strain hardening and WDE performance in terms of incubation period and erosion rate is then studied.

3. Results

3.1. Mechanical properties

3.1.1. Microhardness

The average Vickers microhardness of 17–4 PH stainless steel for each condition along with the standard deviation are shown in Table 3. Condition-A is the softest among the three with 321 $HV_{0.5}$. The aged conditions of H925 and H1025 have relatively high and moderate surface hardness values of 401 and 347 $HV_{0.5}$, respectively. The microhardness values of each condition are close to the ones reported in the literature [29–31]. It is to be noted that the peak hardness of 17–4 PH can be achieved at aging temperature of about 480ºC [30]. As such, condition H925 -being close to the optimum aging treatment- has the greatest hardness. The lower hardness of H1025 compared to H925 could indicate overaging, which is known to reduce the mechanical properties of the 17–4 PH [29,30].

3.1.2. Tensile properties

Table 4 shows the tensile properties obtained for the solution treated condition-A, and H925 and H1025 aged conditions from their engineering stress-strain curves. It can be noticed that the modulus of elasticity (E) is about 195 GPa for both H925 and H1025 aged conditions, whereas Condition-A has a slightly lower value at 187 GPa. This is consistent with Rack et al. [35] results. Moreover, Condition-A has the lowest yield and tensile strengths, which upon aging to H925 results in the highest yield and tensile strengths among the three conditions. H1025 has a relatively intermediate yield and tensile strength. Elastic resilience and strain hardening exponent (n) have also been evaluated for the three conditions of the 17–4 PH steel. The Elastic resilience (which depends on the yield strength and the elastic modulus of the material) is found to be 3.35, 6.68 and 5.65 MJ/m^3 for Condition-A, H925 and H1025, respectively. The strain hardening exponent (n) of Condition-A is the highest among the three conditions at about 0.15 and that of H1025 is the lowest at about 0.02. H925 condition has an intermediate n-value of about 0.06. As discussed in the introduction, elastic resilience and strain hardening exponent will be used in the analysis of erosion results along with the yield strength of each condition. Strength coefficient is used to plot the ideal true stress versus true strain curves as shown in shown in Fig. 3.

True stress-strain curves are plotted for the three conditions of the 17–4 PH using the Hollomon's equation. These curves will be used to interpret the results of the erosion performance. Relevant to analyzing erosion results, is the fracture strength of the materials (last point in each curve). It can be observed from Fig. 3 that the fracture strength of Condition-A is higher than that of H1025, even though Condition-A has lower yield strength value. This is due the high strain hardening exponent value of Condition-A. Condition H925 has the highest fracture strength.

Table 1
Erosion test parameters.

Parameters	Variants
Linear impact speed (m/s)	250, 300
Average droplet size (μm)	460
Impact angle (°)	90
Test chamber pressure (mbar)	30–50
Initial waterline pressure (psi)	30
Waterline pressure during test (psi)	1
Flow rate (liters/min)	0.05

Table 2
Uncertainty range in mass loss and erosion rate.

Impact speed (m/s)	Mass loss accuracy range	Erosion rate accuracy range
250	±2.0 mg	±0.05 mg/min
300	±1.1 mg	±0.05 mg/min

Table 3
Vickers micro-hardness of 17–4 PH stainless steel.

Condition	Average micro-hardness ($HV_{0.5}$)	Standard deviation
Condition-A	321	5.4
H925	401	5.7
H1025	347	4.0

3.2. Erosion performance

The erosion curves of Condition-A versus H925 and Condition-A versus H1025 at impact speed of 250 m/s are shown in Fig. 4 and Fig. 5. Incubation time is estimated from the erosion curve by extending the maximum erosion rate to the ordinate intersection. Condition-A resisted erosion only for about 50 min of WDE exposure in each case, whereas the incubation period was, respectively, about 160 and 75 min long for H925 and H1025. The maximum erosion rate is found to be the same, considering the uncertainty range (Table 2), at about 0.1 mg/min for each condition. A significant difference in the incubation times of H925 and Condition-A (3.2 times) is clearly visible. In contrast, the H1025 condition, despite clearly having greater yield strength and elastic resilience, exhibits a marginally longer incubation (1.5 times) compared to Condition-A. The macrographs in Fig. 6 show the test surface of each sample, which appear to be consistent with the observations from erosion curves.

The erosion curves of Condition-A versus H925 and H1025 at impact speed of 300 m/s are shown in Fig. 7 and Fig. 8. At 300 m/s, the incubation time is the same at about 15 min for Condition-A and H1025, whereas H925 has a greater incubation time of about 21 min. The

Table 4
Tensile properties of 17–4 PH stainless steel in each condition.

Sample condition	Young's modulus (GPa)	0.2% offset Yield strength (MPa)	Tensile strength (MPa)	Strain hardening exponent 'n'	Elastic resilience (MJ/m^3)	Strength Coefficient 'K' (MPa)
Condition-A	187	830	1056	0.15	3.35	1940
H925	195	1257	1324	0.06	6.68	1757
H1025	196	1133	1153	0.02	5.65	1292

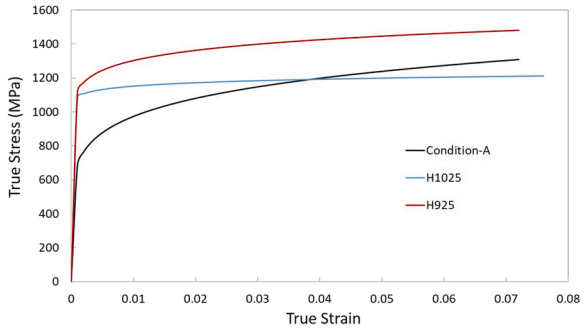

Fig. 3. Ideal true stress versus true strain curves of 17–4 PH stainless steel in each condition.

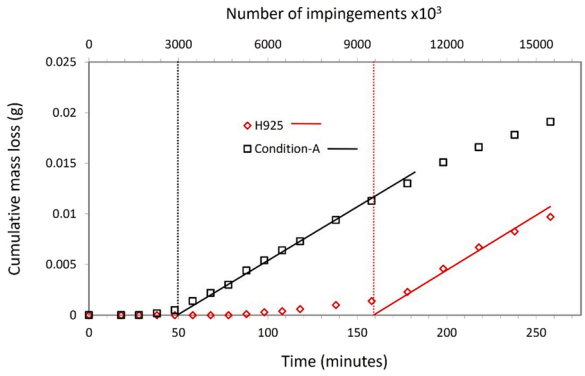

Fig. 4. Erosion curves of Condition-A versus H925 at impact speed of 250 m/s.

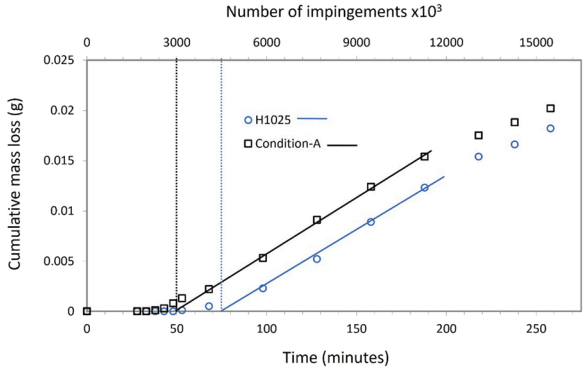

Fig. 5. Erosion curves of Condition-A versus H1025 at impact speed of 250 m/s.

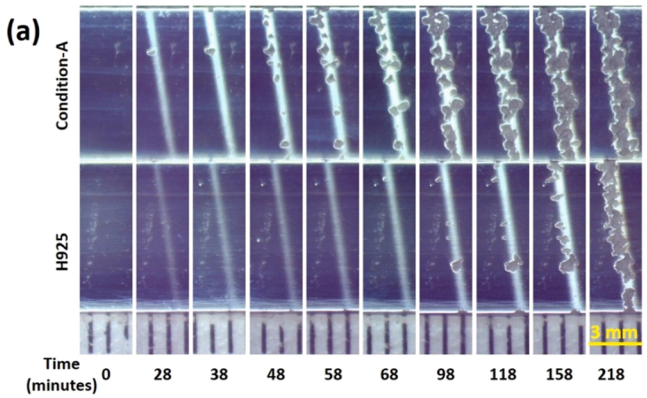

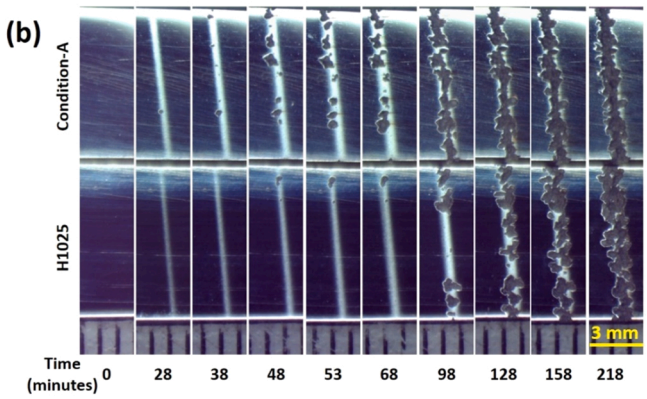

Fig. 6. Macrographs of erosion samples in (a) Condition-A vs H925 and (b) Condition-A vs H1025 tested at impact speed of 250 m/s.

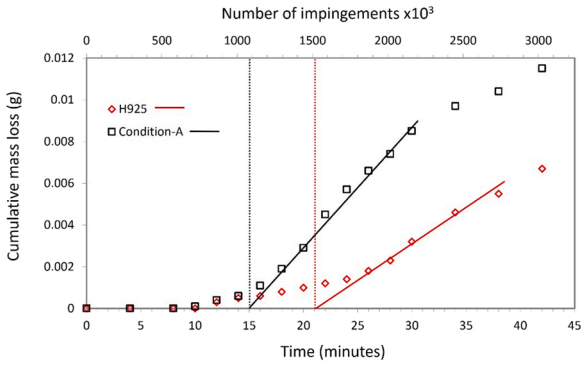

Fig. 7. Erosion curves of Condition-A versus H925 at impact speed of 300 m/s.

maximum erosion rate is about 0.333 mg/min for H925 (Fig. 7), 0.5 mg/min for Condition-A and 0.433 mg/min for H1025 (Fig. 8). The observed results are in accordance with the appearance and evolution of craters seen in the macrographs of Condition-A versus H925 (Fig. 9(a)) and Condition-A versus H1025 (Fig. 9(b)).

The incubation time, number of impingements corresponding to incubation time and the maximum erosion rate for each condition are summarized in Table 5. It is to be noted that the same exposure time results in different number of droplet impingements for WDE tests conducted at different impact speeds. This difference arises due to the different rotational speeds that are used to achieve the desired impact speeds. The number of droplet impingements over a period can be calculated from exposure time using Eq. (1), where the average number of droplet impingements per rotation is 6 droplets per the width of the

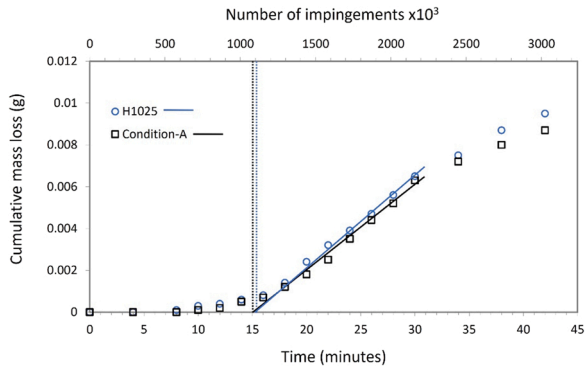

Fig. 8. Erosion curves of Condition-A versus H1025 at impact speed of 300 m/s.

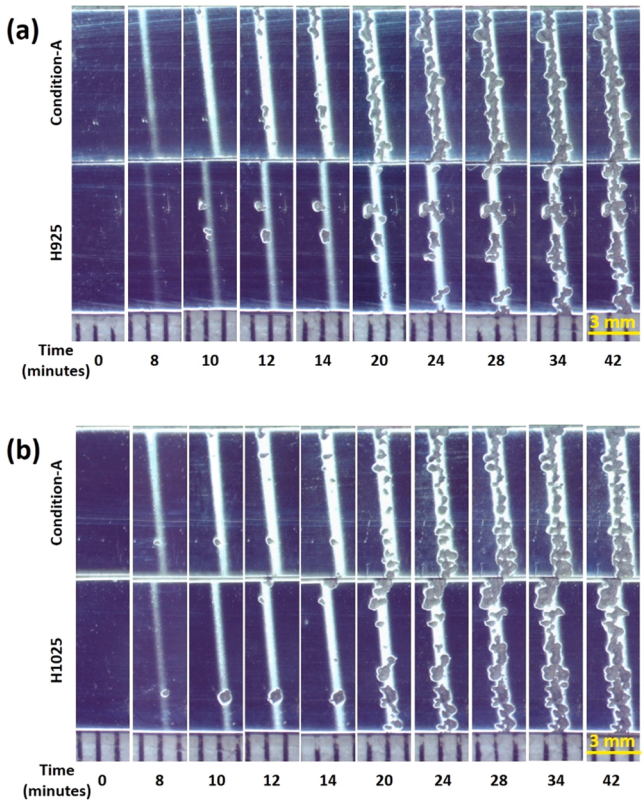

Fig. 9. Macrographs of erosion samples in (a) Condition-A vs H925 and (b) Condition-A vs H1025 tested at impact speed of 300 m/s.

Table 5
Summary of incubation time and maximum erosion rate at 250 and 300 m/s.

Test speed	Condition	Incubation time (minutes)	Number of impingements x10^3	Maximum erosion rate (mg/min)
250 m/s	Condition-A	50	3000	0.107
	H925	160	9600	0.105
	H1025	75	4500	0.112
300 m/s	Condition-A	15	1080	0.5
	H925	21	1512	0.333
	H1025	15.5	1116	0.433

sample (i.e. 8 mm as discussed in the Section 2.4); WDE test speeds of 250 and 300 m/s are achieved at 10,000 and 12,000 RPM respectively; and the exposure time is in minutes.

$$Number \quad of \quad droplets \quad (N_{drop}) = N_{drop/rotation} \times RPM \times time \tag{1}$$

The influence of impact speed on erosion is well established in the literature [12,38]. The acceleration of erosion with increase in impact speed is due to increase in the number of impacts, impact pressures, lateral jetting speeds and the kinetic energy, which are all proportional to impact speed [12]. What is interesting in this work, is the change in the materials' response (in particular the steady-state maximum erosion rate) with the impact speed. Given the uncertainty range, the three conditions of the 17–4 PH steel have nearly identical maximum erosion rate when tested at an impact speed of 250 m/s. However, the variation in the maximum erosion rate between the three conditions becomes appreciable as the impact speed is increased to 300 m/s. This may indicate a change in erosion damage mechanism with the impact speed at this stage of erosion damage.

4. Discussion

The effect of strain hardening exponent as well as the role of mechanical properties (such as hardness, yield and tensile strength, and elastic resilience) on the erosion behavior of the three 17–4 PH conditions are discussed in this section. Prior to that, mechanics of damage accumulation during the incubation period are explained in terms of the true stress-strain curves. This explanation is put forward only to help understand and interpret the role of mechanical properties in the erosion process.

Fig. 10 shows the true stress-strain curves of the three tested conditions of the 17–4 PH, where the yield and fracture points are highlighted. Points A, J and P are the unstrained yield points, whereas F, O, and V are the fracture points of Condition-A, H1025 and H925 respectively. Two important assumptions are made in the present work regarding the impact strain and the accumulation of damage during the incubation period. The first assumption is that, for plastic strain to buildup in the material (and to eventually cause fracture), the portion of droplet impact energy transferred to the material must exceed the elastic resilience of the material in the impact affected region at every impact cycle. In other words, if the transferred impact energy is less than the elastic resilience, plastic deformation (and hence erosion) is avoided, and threshold condition prevails. This is supported by the results of Ibrahim and Medraj [8]. The second assumption is that the incubation period is terminated (and the mass loss begins) when the accumulated plastic strain due to cyclic impact exceeds the fracture strain of the material. Underlining this assumption is the idea that the yield point continuously shifts towards the fracture point by certain magnitude at every single impact due to work hardening. As such, the cyclic time (i.e. cumulative impact energy) needed to reach the fracture point is equivalent to the incubation time. The two assumptions (and hence the

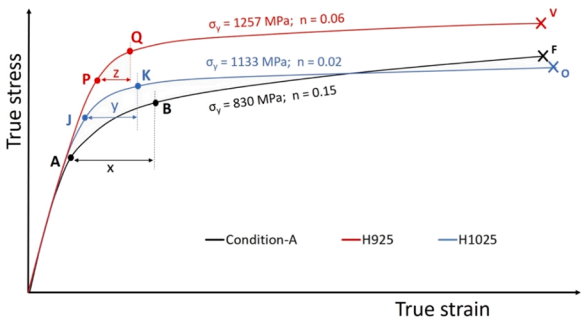

Fig. 10. Schematic explaining the progression of yield point due to strain hardening in each condition of the 17–4 PH stainless steel.

current damage hypothesis) are limited to the end of the incubation period. This is because, as the erosion starts, other factors come into play such as erosion pit and crater shape and dimensions [11]. It is therefore difficult to make such analysis after the start of erosion.

Admittedly, the proposed hypothesis for the incubation period does not take into consideration other phenomena such as crack initiation and propagation and how they lead to material's removal. It also relies on bulk-static properties rather than localized-dynamic properties, which are more representative to the mechanics of water droplet impact. However, in the absence of a comprehensive theory of damage accumulation, this idealization is reasonable in so far as the role of mechanical properties are to be investigated. In the light of this hypothesis, the role of strain hardening and mechanical properties on the erosion process are explored in the ensuing discussion.

4.1. The role of strain hardening

Based on the preceding discussion, the strain hardening exponent (n) can be seen as the main material parameter controlling the damage accumulation process in water droplet erosion. This can be based on two grounds. Firstly, reaching the fracture point in the true stress-strain curve (which represents the end of incubation period) depends on the initial yield point and strain hardening exponent (n) of the material. That is, having high strain hardening exponent results in high fracture strength and hence, longer incubation period. This is evidenced by the observed similarities between the incubation periods of Condition-A and H1025. Although the H1025 condition has significantly larger yield strength compared to Condition-A, they both have very similar fracture strength due to the high strain hardening exponent of Condition-A. This has resulted in almost identical incubation time when both conditions are tested at 300 m/s. Therefore, higher strain hardening exponent results in longer incubation period due to its role in the rate at which the fracture strength is reached.

Secondly, strain hardening exponent influences the length of the incubation period by controlling the cyclic increase in the hardness and yield strength (and the associated elastic resilience) and hence, the rate of damage accumulation. This is because it has been shown that hardness and yield strength of metals increase with exposure to droplet impacts [22]. In other words, every droplet impingement on the surface induces plastic strain in the material, and therefore causes the yield point (i.e. yield strength and strain) to shift towards the fracture point by certain magnitude. For instance, the yield points in Fig. 10 could progressively shift respectively from point A to point B, from J to K, and from P to Q in Condition-A, H1025 and H925 after N cycles (which corresponds to a shift in the true strain values such as x, y, and z for Condition-A, H1025 and H925). Also, as the yield point moves, the elastic resilience at points B, K and Q is greater than that at points A, J and P respectively in Fig. 10. As such, the erosion resistance to each N cycles of droplet impacts is greater than that during the preceding N cycles by the virtue of increased yield strength and elastic resilience. The strain developed is progressively reduced until failure at a rate governed by the n-value of the condition. In other words, it is the strain hardening exponent that governs the continuous progression of yield point, and therefore, controls the rate of erosion damage accumulation. This can be supported by the present results. With Condition-A ($n = 0.15$) as reference, H1025 ($n = 0.02$) has greater yield strength, which is known to increase erosion resistance from the literature, but the erosion performance is similar and the reason is that a lower strain hardening exponent of H1025 leads to lower gains in erosion resistance from work hardening due to droplet impacts. On the other hand, we have Condition-A ($n = 0.15$) as reference against H925 ($n = 0.06$), which has greater yield strength compared to both Condition-A and H1025 (but the yield strength of H925 is relatively closer to that of H1025). The erosion performance of H925 is expected to be better than both Condition-A and H1025. Although this is the case, the 'significantly' better performance of H925 can be explained by its greater yield strength along with its relatively moderate strain hardening capability.

Based on the above analysis, it can be concluded that having greater strain hardening exponent is beneficial to erosion resistance of metals. The greater strain hardening exponent not only results in high fracture strength, but also in higher cyclic yield and elastic resilience, which is conducive to slower rates of impact damage accumulation. This analysis may however not be valid for the cases of already strained materials (e.g. mechanically treated surfaces). This is because, as proposed in [20,27], surface treatments introduce a certain amount of cold working in the material that later results in faster embrittlement and erosion failure. It is expected in such cases that lower strain hardening exponent is conducive to slower rate of damage accumulation and hence longer incubation period. Investigating of the role strain hardening in erosion performance of pre-strained materials is a subject of an ongoing investigation by the present authors.

4.2. The influence of mechanical properties on erosion performance

Although it has been concluded before [2,15,39] that mechanical properties could not -individually- explain the erosion resistance of materials, the potential roles of yield strength, elastic resilience and hardness on the incubation period are discussed in this section. To help visualize the results, the radar chart shown in Fig. 11 is constructed, where the incubation time for the two test speeds (250 and 300 m/s) is plotted against the mechanical properties of the different conditions of the 17–4 PH steel. Fig. 11 indicates that the incubation time increase with yield strength and hardness. However, disproportional relationship is clearly observed between the erosion response and the mechanical properties. For instance, the difference in the yield strength between Condition-A and H925 is only slightly larger than that of Condition-A and H1025. However, the incubation time of H1025 is very close to that of Condition-A at both impact speeds, whereas the incubation time of H925 is significantly longer than that of Condition-A and H1025. The yield strength is reported to play a fundamental role at impact speeds below the threshold condition of the material [8,23] as it could control the plastic deformation, or the lack thereof, of the impacted layer. However, as the end of incubation period necessitates the formation of cracks and localized fracture, bulk yield strength can no longer single-handedly justify the variation in the incubation time between the three conditions of the 17–4 PH steel. The same can be said for the elastic resilience since its value depends on the yield strength and the elastic modulus. It should be remembered that the value of yield strength and elastic resilience of the impact affected region continuously change (with every impingement cycle) during the incubation period according to the stain hardening exponent of the material. As such, their influence

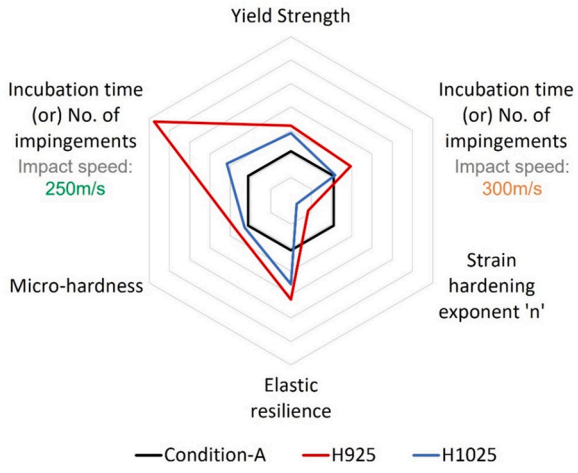

Fig. 11. Radar chart showing mechanical properties and incubation time at 250 and 300 m/s.

on erosion response cannot be quantitatively assessed irrespective of the strain hardening behavior of the material.

As opposed to the yield strength and elastic resilience, the relationship between initial surface microhardness and incubation time exhibits a nearly linear proportionality. That is, Condition-A has a slightly lower hardness compared to that of H1025 (Table 3), while the hardness of H925 is markedly higher than the other two conditions. This is in line with the length of the incubation period of the three conditions. Unlike the strength of the bulk material, hardness controls localized surface deformation. As such, it may be more representative to the surface's resistance to droplet impingements compared to the yield strength and elastic resilience. According to [15,40] hardness is usually a good index to erosion resistance when the same alloy or very similar alloys are tested at different hardness levels. However, erosion resistance of different alloys at the same hardness level may vary by an order of magnitude [40]. Moreover, studies [8,22] have shown that surface hardness continuously changes with cyclic impact during the incubation period due to hardening. This suggests that similar to strength properties, the influence of hardness on the erosion response of the material cannot be accurately studied in isolation from localized hardening behavior. Therefore, it can be confirmed that intrinsic mechanical properties cannot individually account for the erosion resistance, and synergistic combination of properties is needed. It is the suggestion of the present work that such combination must include a stain hardening parameter.

5. Conclusions

In this work, the role of strain hardening in the initial stages of erosion is investigated by studying the erosion performance of 17–4 PH stainless steel in annealed, H925 and H1025 conditions. The samples were tested at impact speeds of 250 and 300 m/s with an average droplet size of 460 μm. In addition to strain hardening exponent, the influence of yield strength, elastic resilience, and hardness on erosion performance is also analyzed. It has been concluded that:

1. At an impact speed of 250 m/s, H1025 has a small difference in incubation time with respect to Condition-A, whereas condition H925 has a significantly longer incubation time. However, at an impact speed of 300 m/s, Condition-A and H1025 have a similar erosion incubation period while H925 has only a slightly improved erosion performance.
2. No change in the maximum erosion rate is observed at 250 m/s impact speed while a slight change in maximum erosion rate is observed at 300 m/s.
3. The different erosion performance of the 17–4 PH steel in the three studied conditions is due mainly to the variation in their mechanical properties as the microstructure is similar for these conditions.
4. The strain hardening exponent is found to play an important role in the erosion performance of the 17–4 PH stainless steel.
5. Hardness and tensile properties such as yield strength, elastic resilience, and fracture strength of each condition synergistically influence the erosion incubation time. Strain hardening exponent is a significant factor in this synergy, because the strain hardening exponent influences the rate of cyclic change in hardness and yield strength due to droplet impacts.

Statement of originality

As corresponding author, I, Prof. Mamoun Medraj, hereby confirm on behalf of all authors that:

i) The paper has not been published previously, that it is not under consideration for publication elsewhere, and that if accepted it will not be published elsewhere in the same form, in English or in any other language, without the written consent of the publisher.

ii) The paper does not contain material which has been published previously, by the current authors or by others, of which the source is not explicitly cited in the paper.

Declaration of Competing Interest

The authors declare that they have no known competing financial interests or personal relationships that could have appeared to influence the work reported in this paper.

Acknowledgements

This work was funded by Natural Sciences and Engineering Research Council, Canada. Discovery Grant ID RGPIN-2018-06789.

References

[1] Di J, Wang S sen, Yan X jiang, Cai L xi, Xie Y hui. Experimental investigation on effect of surface strengthening process and roughness on water droplet erosion behavior in turbomachinery. Tribology Int 2021;153:106647. https://doi.org/10.1016/j.triboint.2020.106647.
[2] Elhadi Ibrahim M, Medraj M. Water droplet erosion of wind turbine blades: mechanics, testing, modeling and future perspectives. Materials 2020;13:157. https://doi.org/10.3390/ma13010157.
[3] Fujisawa K. Effect of impact velocity on time-dependent force and droplet pressure in high-speed liquid droplet impingement. Ann Nucl Energy 2022;166:108814. https://doi.org/10.1016/j.anucene.2021.108814.
[4] Gujba AK, Mahdipoor MS, Medraj M. Water droplet impingement erosion performance of WC-based coating sprayed by HVAF and HVOF. Wear 2021; 484–485:203904. https://doi.org/10.1016/j.wear.2021.203904.
[5] Burson-Thomas CB, Wellman R, Harvey TJ, Wood RJK. Water droplet erosion of aeroengine fan blades: the importance of form. Wear 2019;426–427:507–17. https://doi.org/10.1016/j.wear.2018.12.030.
[6] Zhang Z, Zhang D, Xie Y. Experimental study on water droplet erosion resistance of coatings (Ni60 and WC-17Co) Sprayed by APS and HVOF. Wear 2019;432–433: 202950. https://doi.org/10.1016/j.wear.2019.202950.
[7] Zhang Z, Liu T, Zhang D, Xie Y. Water droplet erosion life prediction method for steam turbine blade materials based on image recognition and machine learning. J Eng Gas Turbines Power 2021;143:1–9. https://doi.org/10.1115/1.4049768.
[8] Ibrahim ME, Medraj M. Prediction and experimental evaluation of the threshold velocity in water droplet erosion. Mater Des 2022;213:110312. https://doi.org/10.1016/j.matdes.2021.110312.
[9] Field JE. ELSI conference: invited lecture. liquid impact: theory, experiment, applications. Wear 1999;233–235:1–12. https://doi.org/10.1016/S0043-1648(99)00189-1.
[10] Marzbali M, Dolatabadi A. High-speed droplet impingement on dry and wetted substrates. Phys Fluids 2020:32. https://doi.org/10.1063/5.0020977.
[11] Adler WF. Mechanics of liquid impact. In: Preece CM, editor. Treatise on materials science and technology, Volume-16. New York: Academic Press, Inc; 1979. p. 127–83. ISBN 012341816X.
[12] Heymann FJ. Survey of clues to the relationship between erosion rate and impact conditions. In: Fyall AA, King RB, editors. Proceedings of the second meersburg conference on rrain erosion and allied phenomena. Federal German Republic: Meersburg; 1967. p. 683–760.
[13] Heymann FJ. On the time dependence of the rate of erosion due to impingement or cavitation. Erosion by cavitation and impingement. ASTM STP-408. Atlantic City, NJ, USA: ASTM,; 1967. p. 70–110. ISBN 978-0-8031-6756-8.
[14] Blowers RM. On the response of an elastic solid to droplet impact. IMA J Appl Math 1969;5:167–93. https://doi.org/10.1093/imamat/5.2.167.
[15] Ahmad M, Schatz M, Casey MV. An empirical approach to predict droplet impact erosion in low-pressure stages of steam turbines. Wear 2018;402–403:57–63. https://doi.org/10.1016/j.wear.2018.02.004.
[16] Seward CR, Pickles CSJ, Marrah R, Field JE. Rain erosion data on window and dome materials. Proc Window Dome Technol Mater III 1992;Vol. 1760:280–90.
[17] Kennedy CF, Field JE. Damage threshold velocities for liquid impact. J Mater Sci 2000;35:5331–9. https://doi.org/10.1023/A:1004842828161.
[18] Thiruvengadam A. The concept of erosion strength. Erosion by cavitation and impingement. ASTM STP-408. Atlantic City, NJ, USA: ASTM; 1967. p. 22–46. ISBN 978-0-8031-6756-8.
[19] Springer, G.S. Erosion by Liquid Impact; 1976;
[20] Gujba AbdullahiK, Hackel L, Medraj M. Water droplet erosion performance of laser shock peened Ti-6Al-4V. Metals 2016;6:262. https://doi.org/10.3390/met6110262.
[21] Ma D, Mostafa A, Kevorkov D, Jedrzejowski P, Pugh M, Medraj M. Water impingement erosion of deep-rolled Ti64. Metals 2015;5:1462–86. https://doi.org/10.3390/met5031462.
[22] Hoff G, Langbein G, Rieger H. Material destruction due to liquid impact. Erosion by cavitation and impingement. ASTM STP-408. Atlantic City, NJ, USA: ASTM; 1967. p. 42–69. ISBN 978-0-8031-6756-8.
[23] Thiruvengadam A, Rudy SL, Gunasekaran M. Experimental and analytical investigations on liquid impact erosion. Characterization and determination of erosion resistance. ASTM STP-474. Atlantic City, NJ, USA: ASTM; 1970. p. 249–87.

[24] Hobbs, J. Experience With a 20-Kc Cavitation Erosion Test. In Erosion by cavitation and impingement. ASTM STP-408; Atlantic City, NJ, USA, 1967; pp. 159–185.
[25] Hancox NL, Brunton JH. The erosion of solids by the repeated impact of liquid drops. Philos Trans R Soc Lond Ser A, Math Phys Sci 1966;260:121–39.
[26] Bowden FP, Brunton JH. The deformation of solids by liquid impact at supersonic speeds. Proc R Soc Lond A Math Phys Sci 1961;263:433–50.
[27] Thomas GP, Brunton JH. Drop impingement erosion of metals. Proc R Soc Lond Ser A Math Phys Sci 1970;314:549–65.
[28] ASTM A693-06. Standard specification for precipitation-hardening stainless and heat-resisting steel plate, sheet, and strip. two thousand sixth ed. West Conshohocken, PA, USA: ASTM International; 2006.
[29] Viswanathan UK, Banerjee S, Krishnan R. Effects of aging on the microstructure of 17-4 PH stainless steel. Mater Sci Eng 1988;104:181–9. https://doi.org/10.1016/0025-5416(88)90420-X.
[30] Hsiao CN, Chiou CS, Yang JR. Aging reactions in a 17-4 PH stainless steel. Mater Chem Phys 2002;74:134–42. https://doi.org/10.1016/S0254-0584(01)00460-6.
[31] Yeli G, Auger MA, Wilford K, Smith GDW, Bagot PAJ, Moody MP. Sequential nucleation of phases in a 17-4PH steel: microstructural characterisation and mechanical properties. Acta Mater 2017;125:38–49. https://doi.org/10.1016/j.actamat.2016.11.052.
[32] Kirols HS, Kevorkov D, Uihlein A, Medraj M. The effect of initial surface roughness on water droplet erosion behaviour. Wear 2015;342–343:198–209. https://doi.org/10.1016/j.wear.2015.08.019.
[33] ASTM E8/E8M - 13a. Standard test methods for tension testing of metallic materials. two thousand thirteenth ed. West Conshohocken, PA, USA: ASTM International,; 2013.
[34] Datsko J. Materials selection for design and manufacturing: theory and practice. Marcel Dekker Inc,; 1997. ISBN 9780824798444.
[35] Rack HJ, Kalish D. Strength, fracture toughness, and low cycle fatigue behavior of 17-4 Ph stainless steel. Metall Trans 1974;5:1595–605. https://doi.org/10.1007/BF02646331.
[36] ASTM G73-10. Standard test method for liquid impingement erosion using rotating apparatus. West Conshohocken, PA, USA: ASTM International,; 2017.
[37] Ahmad M, Casey M, Sürken N. Experimental assessment of droplet impact erosion resistance of steam turbine blade materials. Wear 2009;267:1605–18. https://doi.org/10.1016/j.wear.2009.06.012.
[38] Mahdipoor MS, Kirols HS, Kevorkov D, Jedrzejowski P, Medraj M. Influence of impact speed on water droplet erosion of TiAl compared with Ti6Al4V. Sci Rep 2015;5:1–17. https://doi.org/10.1038/srep14182.
[39] Heymann FJ. Erosion by liquids. Mach Des 1970;10:118–24.
[40] Hammitt, FG, Heymann, F.J. Liquid Erosion Failures. In ASM Handbook, Volume-11; 1986; pp. 163–171.